JGR Atmospheres

RESEARCH ARTICLE
10.1029/2021JD035702

H_2O_2 and CH_3OOH (MHP) in the Remote Atmosphere: 2. Physical and Chemical Controls

Hannah M. Allen[1], Kelvin H. Bates[2], John D. Crounse[3], Michelle J. Kim[3], Alexander P. Teng[3], Eric A. Ray[4,5], and Paul O. Wennberg[3,6]

[1]Division of Chemistry and Chemical Engineering, California Institute of Technology, Pasadena, CA, USA, [2]School of Engineering and Applied Sciences, Harvard University, Cambridge, MA, USA, [3]Division of Geological and Planetary Sciences, California Institute of Technology, Pasadena, CA, USA, [4]Cooperative Institute for Research in Environmental Sciences (CIRES), University of Colorado, Boulder, CO, USA, [5]Earth System Research Laboratory, National Oceanic and Atmospheric Administration, Boulder, CO, USA, [6]Division of Engineering and Applied Science, California Institute of Technology, Pasadena, CA, USA

This article is a companion to Allen et al. (2021), https://doi.org/10.1029/2021JD035701.

Key Points:

- The global distribution of H_2O_2 and methyl hydroperoxide (MHP) reflects the influence of photochemistry, convective transport, and wet and dry deposition
- Deposition of H_2O_2 plays a key role in removing HO_x within the marine boundary layer
- MHP in the upper troposphere is highly sensitive to convective transport and the Goddard Earth Observing System (GEOS)-Chem model substantially underestimates MHP advective mass fluxes

Supporting Information:

Supporting Information may be found in the online version of this article.

Correspondence to:

H. M. Allen and P. O. Wennberg,
hallen@caltech.edu;
wennberg@caltech.edu

Citation:

Allen, H. M., Bates, K. H., Crounse, J. D., Kim, M. J., Teng, A. P., Ray, E. A., & Wennberg, P. O. (2022). H_2O_2 and CH_3OOH (MHP) in the remote atmosphere: 2. Physical and chemical controls. *Journal of Geophysical Research: Atmospheres*, *127*, e2021JD035702. https://doi.org/10.1029/2021JD035702

Received 13 AUG 2021
Accepted 27 FEB 2022

Abstract Hydrogen peroxide (H_2O_2) and methyl hydroperoxide (MHP, CH_3OOH) serve as HO_x (OH and HO_2 radicals) reservoirs and therefore as useful tracers of HO_x chemistry. Both hydroperoxides were measured during the 2016–2018 Atmospheric Tomography Mission as part of a global survey of the remote troposphere over the Pacific and Atlantic Ocean basins conducted using the NASA DC-8 aircraft. To assess the relative contributions of chemical and physical processes to the global hydroperoxide budget and their impact on atmospheric oxidation potential, we compare the observations with two models, a diurnal steady-state photochemical box model and the global chemical transport model Goddard Earth Observing System (GEOS)-Chem. We find that the models systematically under-predict H_2O_2 by 5%–20% and over-predict MHP by 40%–50% relative to measurements. In the marine boundary layer, over-predictions of H_2O_2 in a photochemical box model are used to estimate H_2O_2 boundary-layer mean deposition velocities of 1.0–1.32 cm s^{-1}, depending on season; this process contributes to up to 5%–10% of HO_x loss in this region. In the upper troposphere and lower stratosphere, MHP is under-predicted and H_2O_2 is over-predicted by a factor of 2–3 on average. The differences between the observations and predictions are associated with recent convection: MHP is under-estimated and H_2O_2 is over-estimated in air parcels that have experienced recent convective influence.

Plain Language Summary Hydrogen peroxide (H_2O_2) and methyl hydroperoxide (MHP, CH_3OOH) in the atmosphere can act as reservoirs for one of the main drivers of atmospheric chemistry, HO_x (HO_x = OH and HO_2). Both H_2O_2 and MHP were measured during the 2016–2018 Atmospheric Tomography Mission (ATom), which investigated the atmosphere over the oceans far from direct human influence. The measurements are compared to two types of models to assess our understanding of the chemical and physical processes that control their abundance. We find that these models consistently predict H_2O_2 to be lower and MHP to be higher than was measured during ATom. We use the discrepancy between the model and the measurements to investigate the role of deposition (removal of compounds from the Earth's atmosphere due to interactions with surfaces and with liquid water) on H_2O_2 in the lowest portion of atmosphere and the role of convection (vertical transport during storms and other meteorological events) on MHP between 6 and 12 km altitudes.

1. Introduction

Hydrogen peroxide (H_2O_2) and methyl hydroperoxide (MHP, CH_3OOH) are of key importance in the atmosphere because they reside at the center of the cycling of the atmosphere's main oxidant HO_x (OH and HO_2 radicals). They are both reservoirs of HO_x due to their formation from HO_x chemistry and reformation of HO_x upon further photooxidation. H_2O_2 is formed in the atmosphere primarily via the HO_2 self-reaction:

$$HO_2 + HO_2 \rightarrow H_2O_2 + O_2 \quad (1)$$

Whereas MHP arises primarily via the reaction of HO_2 with the methyl peroxy radical (MPR, CH_3OO). MPR is formed via the oxidation of methane (CH_4) by OH:

$$CH_4 + OH \rightarrow CH_3OO + H_2O \quad (2)$$

$$CH_3OO + HO_2 \rightarrow CH_3OOH + O_2 \quad (3)$$

The photochemistry of other larger organic molecules, such as acetone, can also lead to MPR and subsequently MHP formation. The formation of H_2O_2 and MHP is inversely related to the abundance of NO and mostly occurs in low to moderate NO_x (NO and NO_2) environments. High NO_x limits hydroperoxide production because NO competes with HO_2 for reaction with the peroxy radical precursors (HO_2 and MPR) to instead form either OH (for HO_2) or CH_3O (which decomposes to HCHO and HO_2 in the presence of O_2). The abundance of H_2O_2 and MHP is thus indicative of a key branching in the oxidative chemistry of the troposphere: whether peroxy radicals react with HO_2 leading to radical termination or react with NO leading to radical propagation. This branching has particular consequences for atmospheric odd oxygen (O_x, comprising O_3 and the compounds with which it rapidly cycles such as NO_2, NO_3, etc.) as the former leads to loss of O_x whereas the later leads to production of O_x.

Both H_2O_2 and MHP undergo photochemical loss via photolysis or reaction with OH that return HO_x to the atmosphere. For H_2O_2, these losses are:

$$H_2O_2 + h\nu \rightarrow 2OH \quad (4)$$

$$H_2O_2 + OH \rightarrow HO_2 + H_2O \quad (5)$$

For MHP, these losses directly return HO_x as well as form formaldehyde (HCHO) which may further react to return HO_x to the atmosphere.

$$CH_3OOH + h\nu \rightarrow CH_3O + OH \quad (6)$$

$$CH_3O + O_2 \rightarrow HCHO + HO_2 \quad (7)$$

$$CH_3OOH + OH \xrightarrow{\sim 0.7} CH_3OO + H_2O \quad (8)$$

$$\xrightarrow{\sim 0.3} HCHO + OH + H_2O \quad (9)$$

The branching ratio of the MHP + OH reaction varies between 0.65 and 0.83 in favor of abstraction at the hydroxy hydroperoxide leading to CH_3OO formation, with a recommended average of 0.70 (Anglada et al., 2017; Atkinson et al., 2006; Niki et al., 1983; Vaghjiani & Ravishankara, 1989). For both hydroperoxides, photolysis recycles HO_x and results in a net of no change to total HO_x while reaction with OH is net oxidant consuming. Formation and subsequent photolysis of H_2O_2 converts HO_2 to OH, similar to the reaction of HO_2 with NO, with an important difference being that the former does not lead to O_3 production. However, hydroperoxide photochemical loss may not occur in the same region as their formation, resulting in transport of HO_x to areas that may have very different chemical regimes. For example, Jaeglé et al. (2000) found that convective transport moves MHP from a region of generally low NO to the mid and upper troposphere where NO levels are higher, leading to higher O_x production.

H_2O_2 and MHP are also subject to loss through wet and dry deposition that removes these HO_x reservoirs from the atmosphere, likely permanently. Deposition is parameterized as two distinct processes: dry deposition, which is the removal of gases or particles from the atmosphere due to impaction onto land and ocean surfaces following turbulent transfer; and wet deposition, which occurs when gases are incorporated into suspended liquid water either by in-cloud scavenging or by washout from falling precipitation. Depositional loss depends not only upon the chemical properties of the gas, such as solubility, but also upon a variety of factors including the planetary boundary layer height, surface properties (e.g., area, roughness, moisture content, etc.), cloud liquid water content, and meteorological parameters such as vertical wind speed (Chang et al., 2004; Hall & Claiborn, 1997; Jobson et al., 1998; Nguyen et al., 2015; Walcek, 1987). Due to its high solubility, H_2O_2 is particularly susceptible to depositional losses while the less soluble MHP is affected significantly less (Lee et al., 2000). Hydroperoxide loss by deposition represents a net loss of oxidant as H_2O_2 and MHP are removed with no return of HO_x to the atmosphere.

In addition to photochemical and depositional loss, hydroperoxides alter the atmosphere's oxidative potential via their transport in, for example, convective activity (Figure 1). Convection occurs when parcels of air become unstable with respect to vertical transport; with strong enough convection, large towering cumulus clouds form that can penetrate deep into the upper troposphere and lower stratosphere (UTLS, typically 8–12 km). Because

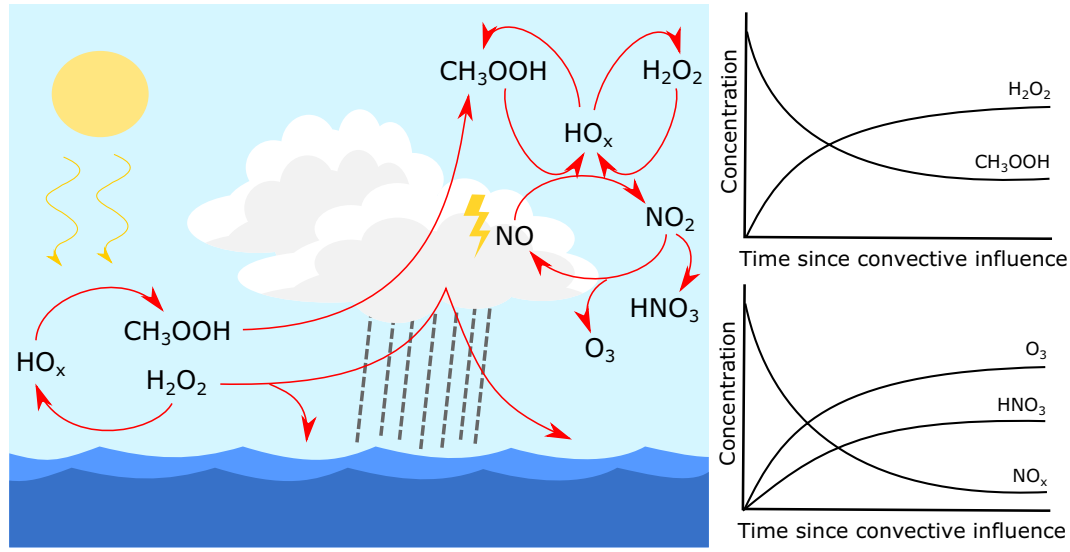

Figure 1. Simplified schematic of hydroperoxide cycling in the remote atmosphere. (Left) In the lower troposphere, generation of HO_x forms H_2O_2 and methyl hydroperoxide (MHP) that cycle back to HO_x with photochemical reactions. H_2O_2 readily undergoes deposition, removing it from the atmosphere under both wet and dry conditions. MHP is less soluble and therefore may be lofted to the upper troposphere and lower stratosphere (UTLS) during convection events, where it participates in HO_x and NO_x (e.g., from lightning) chemistry. (Right) Schematic reflecting the changes in peroxide, NO_x, HNO_3, and O_3 relative mixing ratios following convection to the UTLS.

MHP and H_2O_2 have different solubilities, the ratio of these two compounds can be used as a metric to identify areas with recent convective activity (see, e.g., Snow et al., 2007). H_2O_2 and MHP have similar mixing ratios in the boundary layer (H_2O_2/MHP ~1–3), but H_2O_2 is preferentially removed by cloud water (high scavenging efficiency) and precipitation that forms during convection while MHP is lofted with minimal loss (low scavenging efficiency) (Barth et al., 2016; Bela et al., 2018; Cuchiara et al., 2020; Heikes et al., 1996; O'Sullivan et al., 1999). The scavenging efficiency of these hydroperoxides depends upon the interactions of these species with the environment as they are lofted: interactions with the freezing and/or evaporation of cloud particles may lead to less efficient scavenging of H_2O_2 and/or more efficient scavenging of MHP (Bela et al., 2016; Bozem et al., 2017; Y. Li et al., 2019). Following convection, MHP in the UTLS may be enhanced by 3–6 times background levels (Cohan et al., 1999; Jaeglé et al., 2000; Ravetta et al., 2001).

Overall, the influence of these compounds on the UTLS due to convective transport lasts on order of 3–10 days based on the lifetime of MHP and H_2O_2 and the subsequent relaxation to local steady-state (Bertram et al., 2007; Jaeglé et al., 1997). However, in that time MHP may be photolyzed or oxidized to produce HO_x and therefore the net influence of convective transport of MHP may be to increase HO_x levels in the UT. For example, MHP photolysis may contribute 20%–40% of HO_x production in convective outflow, compared with just 3%–10% in background UTLS air (Cohan et al., 1999; Jaeglé et al., 2000; Prather & Jacob, 1997; Ravetta et al., 2001). Through transport via convection and subsequent photochemistry, hydroperoxides can facilitate the effective transport of HO_x from the lower atmosphere to the upper atmosphere and thereby significantly increase the HO_x abundance in the latter. Accurate parameterization of convective transport of trace gases is a well-known challenge in models as the efficiency of such transport depends on the details of many poorly quantified aspects of convection, such as entrainment and detrainment rates, cloud water size distribution, vertical velocities, etc (Lawrence & Rasch, 2005; Zhang et al., 2021).

In this study, the chemical and physical controls on global hydroperoxide mixing ratios are assessed through comparisons between global seasonal measurements and photochemical models. The data collection methodology and global hydroperoxide distribution are outlined in a companion paper (Allen et al., 2021). Here, we discuss the relative importance of photochemistry in setting hydroperoxide distributions from nearly pole-to-pole over the Atlantic and Pacific oceans. We investigate the role of physical processes on the distribution of H_2O_2 and MHP, including estimating the rate of H_2O_2 deposition in the marine boundary layer needed to reconcile observations with box model predictions. Finally, we use Goddard Earth Observing System (GEOS)-Chem, a

global chemical transport model, to investigate the role of convection in lofting hydroperoxides and their impact on the UTLS.

2. Methods

2.1. Field Deployment: Atmospheric Tomography Mission

Global observations of H_2O_2 and MHP were made during the Atmospheric Tomography (ATom) Mission, which used the NASA DC-8 to collect atmospheric vertical profiles of trace gases and aerosols in the remote atmosphere. The deployments were scheduled to sample each season: ATom-1 in August 2016 (29 July 2016–23 August 2016), ATom-2 in February 2017 (26 January 2017–21 February 2018), ATom-3 in October 2017 (28 September 2017–27 October 2017), and ATom-4 in May 2018 (24 April 2018–21 May 2018). Each deployment consisted of 11–13 flights that followed a prescribed flight track spanning latitudes between −85° and 85° by first traveling southbound over the Pacific Ocean and then traveling northbound over the Atlantic Ocean. During each flight, the aircraft underwent continuous ascents and descents to gather vertical profiles ranging from altitudes of about 180 m above the ocean to just under 13,500 m. Hydroperoxides were measured using the CIT-CIMS, which combines a time-of-flight and a triple quadrupole chemical ionization mass spectrometer using CF_3O^- ion chemistry to sensitively detect gas-phase atmospheric hydroperoxides. ATom primarily resulted in data collected over the remote ocean, but did include periods over land due to flight requirements; the data presented here have been filtered to exclude the measurements collected over land. The ATom Mission and CIT-CIMS technique are discussed in much further detail in the companion paper (Allen et al., 2021).

2.2. GEOS-Chem

Observations of atmospheric hydroperoxide mixing ratios from ATom were compared to those predicted by the global transport model GEOS-Chem. GEOS-Chem is a three-dimensional atmospheric chemistry model driven by meteorological data from radio sondes and satellite observations of the Earth's land surface, atmosphere, ocean, and biogenic parameters (Bey et al., 2001; Bian & Prather, 2002; Keller et al., 2014; Lin & Rood, 1996). The GEOS-Chem chemical module simulates atmospheric concentrations of various species taking into account emissions, transport, chemistry, aerosol microphysics, and deposition (Harvard, 2019). Further details on the chemical and physical mechanisms used in the GEOS-Chem simulations are given in the Supporting Information. The meteorological data are assimilated from the GEOS of the NASA Global Modeling and Assimilation Office (GMAO). GEOS-Chem integrates the meteorological data using the GEOS Forward Processing (GEOS-FP) data archive with a native resolution of 0.25° latitude by 0.325° longitude and 72 vertical atmospheric layers and a 3-hr temporal resolution (1-hr for surface data).

In this study, GEOS-Chem simulations were conducted for 2016–2018, with a 1-year spin up, using GEOS-Chem v11-2d at 2° × 2.5° latitude-longitude grid resolution using the GEOS-FP meteorology archive. The model was updated with $CH_3OO + OH$ chemistry ($k = 1.6 \times 10^{-10}$ cm^3 s^{-1}), as well as with improvements to certain emissions inventories, as described in Bates et al. (2021). Sensitivity studies were conducted on the rate of HO_2 loss on heterogenous surfaces by altering the uptake coefficient (γ, Stone et al., 2012), on MHP wet scavenging by altering the MHP Henry's Law Coefficient, and on the rate of the $CH_3OO + OH$ reaction by altering the rate coefficient to assess the impact of this chemistry on the hydroperoxide budget (see below and the Supporting Information). GEOS-Chem results are presented in two forms: one in which model times and locations are matched to the flight campaign data at 2 min temporal resolution and one in which ocean basin curtains are generated using a monthly averaged output of each deployment that is centered on either −170° longitude (Pacific Ocean) or −25° longitude (Atlantic Ocean).

2.3. Photochemical Box Model

A zero-dimensional diurnal photochemical box model is used to evaluate the measurements of hydroperoxides against their concentrations as predicted at pseudo-steady-state. The box model contains a detailed mechanism for remote tropospheric HO_x-NO_x-VOC chemistry that uses over 35 chemical species and 85 reactions. The model does not include physical processes such as heterogeneous chemistry (e.g., HO_2 loss on aerosols is not included), transport, or wet or dry deposition. Data used for analysis have been filtered such that the rate of NO_2 photolysis

at each point is greater than 1×10^{-3} s^{-1}, ensuring only measurements collected in daylight are used. Compounds included in the model are either initiated with measured values when available or calculated from steady-state with parameters such as temperature, pressure, and H_2O mixing ratio are constrained to their observed values.

Data used to initiate the model includes measurements of OH and HO_2 (uncertainties of ±35%, Brune, Miller, and Thames, 2019); photolysis rates (uncertainties of ±15%, Hall and Ullmann, 2019); H_2O_2, MHP, HO_2NO_2, and HNO_3 (uncertainties of ±30%, ±30%, ±30%, and ±30%, respectively, Allen et al., 2019); H_2O (uncertainties of ±5%, Diskin and DiGangi, 2019); peroxyacyl nitrates (PAN, uncertainties of ±20%, Huey et al., 2019); HCHO (uncertainties of ±10%, Hanisco et al., 2019); CH_4 and CO (uncertainties of ±0.7 ppb and ±3.6 ppb, respectively, McKain and Sweeney, 2018); NO, NO_2 and O_3 (uncertainties of ±0.03%–100%, ±0.06%–100%, and ±0.03%, respectively, Ryerson et al., 2019); PAN (uncertainties of ±0.06%–100%, Elkins et al., 2019); and acetone ($CH_3C(O)CH_3$, uncertainties of ±20%, Apel et al., 2019); as well as temperature and pressure. The model data for August (ATom-1) is limited by the availability of peroxyacetic nitrate (PAN) measurements, leading to high uncertainty at the most poleward extremes.

Using the observations as an initial point, the model calculates the diurnally varying production and loss of each chemical species over the course of 120 simulated hours. Photolysis rates for relevant species are calculated using actinic flux with cross sections and quantum yields from Burkholder et al. (2015). The actinic flux is produced from the Tropospheric Ultraviolet and Visible (TUV) radiation model (NCAR), which utilizes inputs of temperature, pressure, ozone column, and altitude to determine cloud-free actinic fluxes at the latitude, longitude, altitude, and time of year of the ATom measurements. Comparisons of model-generated photolysis rates with those available from actinic flux measurements using the Charged-coupled device Actinic Flux Spectroradiometers (CAFS) onboard indicate good agreement between the two and modeled photolysis rates have been scaled to match CAFS observations where available. Chemical rates are similar to those used in GEOS-Chem and calculated using temperature-dependent rate constants from Burkholder et al. (2015), including a temperature dependent rate constant of $3.7 \times 10^{-11}\exp(350/T)$ for $CH_3OO + OH$ chemistry (Jenkin et al., 2019). From the TUV-generated actinic flux of a 24-hr solar cycle, the box model calculates a 5-day diurnal pattern of compound mixing ratios at each point along the flight track. Five days was chosen because the concentrations of most compounds have reached steady-state (i.e., concentrations were invariant over multiple days) within this time frame.

3. Results and Discussion

3.1. Hydroperoxide Lifetime and Photochemistry

During ATom, H_2O_2 mixing ratios were highest in the lower troposphere within the tropical and subtropical latitudes, regions that typically exhibited high HO_x-formation and generally lower NO concentrations. Based on box model predictions, the highest production of H_2O_2 from HO_2 self-reaction occurs within latitudes of −10° to 20°, driven by the highest UV fluxes, and quickly falls off poleward. Similarly, the highest production of H_2O_2 from the HO_2 self-reaction occurs within the boundary layer and lower troposphere (<2 km altitude) and quickly declines with increasing altitude. The highest estimated rate of H_2O_2 production from this chemistry occurred in the October deployment (ATom-3) with an average rate of 7.1×10^{-4} s^{-1}, or 1.3 ppb per day while the lowest occurred during the February deployment (ATom-2) with an average production rate of 4.3×10^{-4} s^{-1} or 0.6 ppb per day. However, H_2O_2 also forms in regions where other factors such as biomass burning drive high HO_x and VOC concentrations that lead to higher mixing ratios of this hydroperoxide (see Allen et al., 2021).

Similarly, H_2O_2 photochemical loss occurs in regions with strong photochemical activity, primarily in the boundary layer of the tropical and subtropical latitudes. H_2O_2 photolysis tends to comprise more than half the photochemical H_2O_2 loss (loss due to deposition is discussed in detail in the following section) with the remainder accounted for by OH reaction (Figure 2). On average, reaction with OH is 30%–35% of H_2O_2 photochemical loss with global minimums of 2%–6% and maximums of 63%–75%, depending on season, due to the slower average OH loss rate (calculated using the $H_2O_2 + OH$ rate constant from Burkholder et al. (2015) and measured [OH], $\sim 3.6 \times 10^{-6}$ s^{-1}) and more than twice as fast average photolysis rate (calculated using the box model, $\sim 9.0 \times 10^{-6}$ s^{-1}). The relative contribution of OH to H_2O_2 loss has a slight dependence on latitude and season but mostly shows variation depending on altitude. The average contribution of OH reaction to H_2O_2 loss is higher at lower altitudes (40%–45% on average) and decreases at higher altitudes (20%–25% on average), although some variation does exist above 12 km (e.g., ATom-3) likely due to overall less data collected at the highest altitudes. ATom observa-

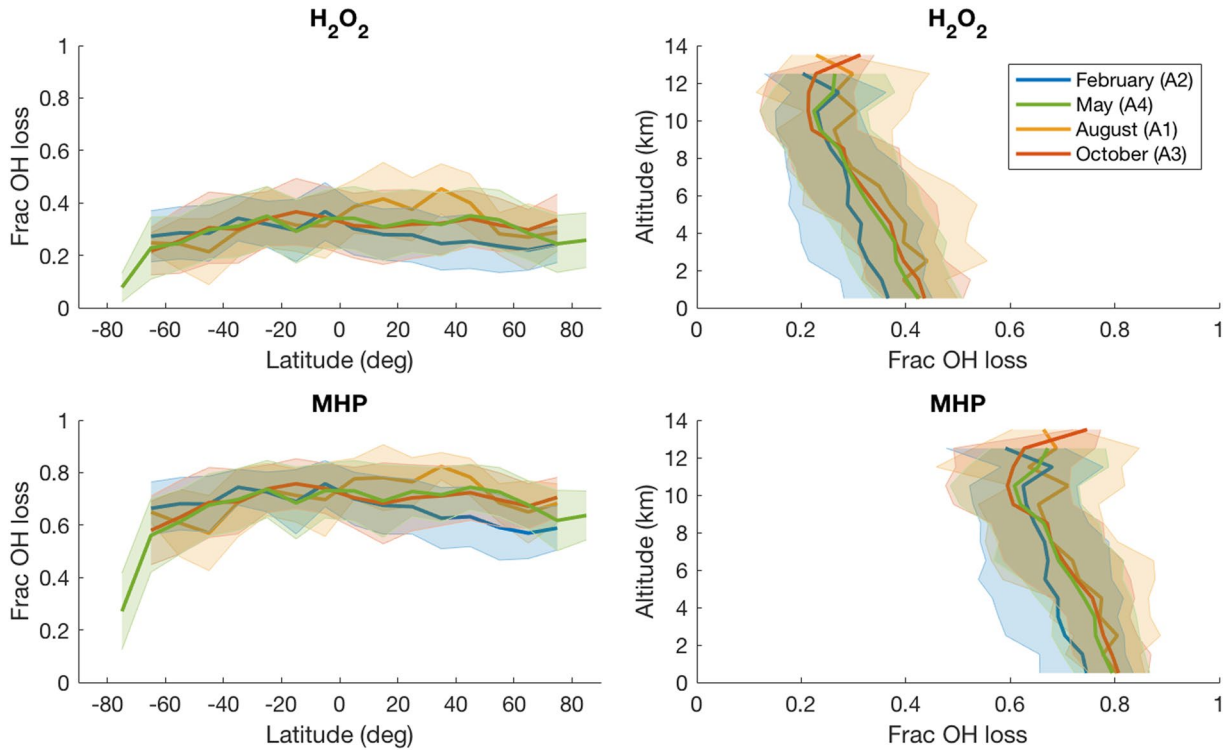

Figure 2. Fraction of OH loss relative to photolysis (OH/(OH + *hv*)) for H_2O_2 and MHP across latitude bins (averaging all altitudes) and altitude bins (averaging all latitudes) for all four deployments of ATom as predicted by a photochemical box model. A1–A4 refers to the four different ATom deployments. Shading represents one sigma standard deviation of the mean.

tions show OH mixing ratios decline with altitude in the tropics but are fairly consistent with altitude outside this region (Brune, Miller, Thames, et al., 2019), while the increased radiation at higher altitudes leads to increasing photolysis rates in the upper atmosphere (Travis et al., 2020). These observations suggest the altitude dependence of relative H_2O_2 loss is likely due to the changes in radiation increasing photolysis rates. Because H_2O_2 photolysis conserves HO_x while loss to OH represents a net loss of HO_x, areas with a high ratio of H_2O_2 loss to OH indicate regions that are net oxidant consuming.

The relative contribution of OH to the overall MHP photochemical loss (OH/(OH + *hv*)) exhibits latitudinal and altitudinal patterns very similar to that of H_2O_2. As shown in Figure 2, MHP loss to OH comprises a higher percentage of MHP photochemical loss than H_2O_2 + OH does of H_2O_2 photochemical loss. During the ATom deployments, the average rate of photolysis was 7.3×10^{-6} s^{-1} while the average rate of OH loss was nearly twice as fast at 15×10^{-6} s^{-1}, leading to a much higher fraction of MHP loss to OH than to photolysis. The average global value of MHP loss to OH varies from 66% (February, ATom-2) to 72% (August, ATom-1), with minimums of 12%–25% and maximums of 90%–95%, depending on season. This average percentage contribution of OH to photochemical loss shows a very slight dependence on latitude and altitude. Loss to OH is typically highest in the tropical and subtropical region and decreases moving poleward and typically highest at low altitudes (contributing about 80%) and decreases with increasing altitude (to an average of 65%). Note that prior to running the model, points along the flight track in which NO_2 photolysis was below 1×10^{-3} s^{-1} were excluded, leading to some potential biases in the poleward extremes. MHP may undergo deposition as well, but due to the relatively low Henry's Law constant of MHP this loss is not nearly as important as it is for H_2O_2.

The lifetime of H_2O_2 with respect to photochemical loss is 21 hr (daytime) on average and spans the range from just a few hours (4–8) to several hundred (>100) depending on season and latitude. The H_2O_2 lifetime shows little dependence on altitude but a strong dependence on latitude due to the variation in UV actinic flux. The H_2O_2 photochemical lifetime is shortest in the equatorial region and increases moving poleward. Similarly, the global average photochemical lifetime of MHP in the atmosphere is around 11 hr (daytime) and varies considerably between 1 and 3 hr to much longer (>50 hr) depending on atmospheric region. Like H_2O_2, MHP photochemical

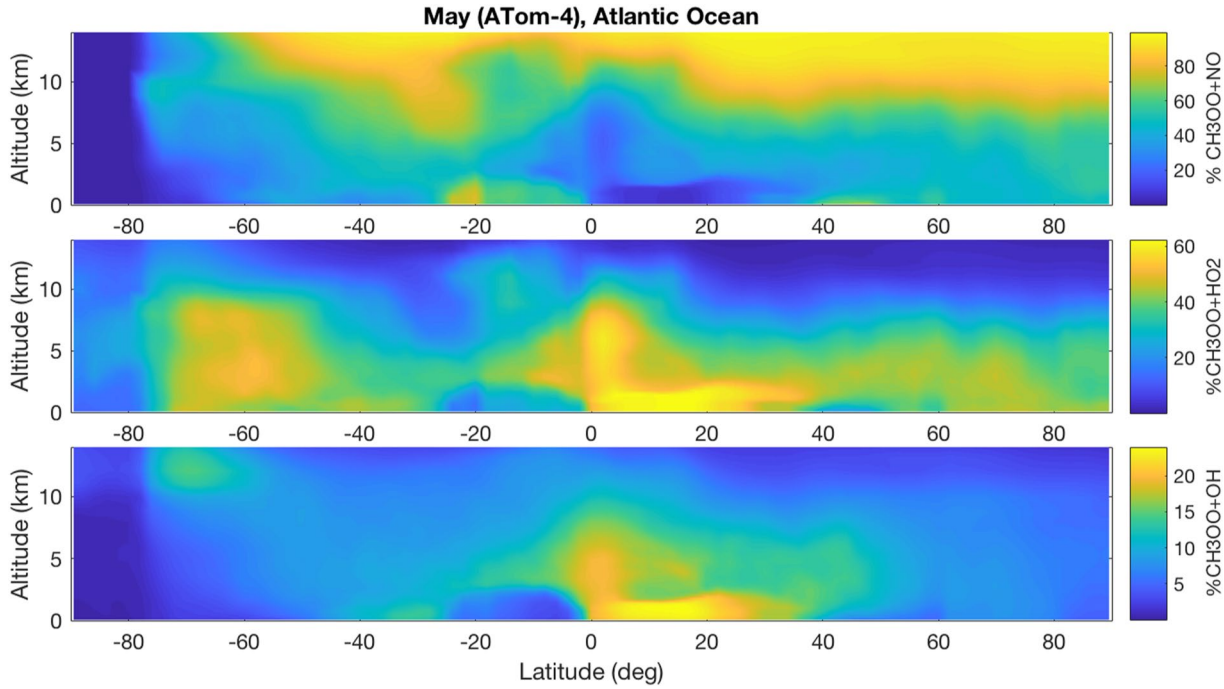

Figure 3. Fraction of CH_3OO that reacts with NO (top), HO_2 (middle), or OH (bottom) across latitude and altitude for the Atlantic Ocean basin during the May deployment (ATom-4) as predicted by Goddard Earth Observing System-Chem. Regions with high $CH_3OO + HO_2$ produce MHP and are net oxidant consuming. Note the different color bar scaling factors in each panel.

lifetime does not vary significantly with altitude but does show a latitudinal dependence due to sunlight. The MHP lifetime is shortest in the tropics and subtropics and increases moving poleward. While the H_2O_2 photochemical lifetime is longer than that of MHP, H_2O_2 is subject to much larger non-photochemical losses (NPLs) than MHP and thus the overall lifetime of these two species in the atmosphere is similar when physical losses are taken into account.

In addition to H_2O_2 and MHP lifetime, the GEOS-Chem simulation reveals the distribution of atmospheric regions that are dominated by either HO_x or NO_x chemistry. Figure 3 compares the fraction of MPR that reacts with NO, HO_2, or OH in the Atlantic Ocean basin for the May (ATom-4) deployment. ATom-4 is fairly representative of reaction patterns across the deployments and ocean basins with some enhancement in either the tropics or mid-latitudes depending on season and basin (see the Supporting Information). These reactions show some latitudinal dependence; MPR + OH is localized to the tropical regions while MPR + HO_2 is prominent in the tropics but occurs in the mid-latitude regions as well. However, these reactions have a stronger altitudinal dependence. In the lowest portion of the atmosphere, HO_2 contributes up to 60% of CH_3OO loss while reaction with OH contributes up to 25% of CH_3OO loss as this is a very photochemically active region with higher HO_x production. The contribution of HO_2 to MPR reactions decreases with increasing altitude and declines to <10% in the upper troposphere (>8 km) as HO_x declines and NO becomes more prominent due to additions of NO_x from lightening and the increase in the lifetime of NO_x due to the lower O_3 mixing ratios. Hence this strong gradient with altitude correlates well with the expected distribution of both HO_x and NO_x sources. The impact of CH_3OO + OH on MHP production will be further explored in Section 3.3.

3.2. H_2O_2 Deposition in the Marine Boundary Layer

NPL of H_2O_2 is estimated here by comparing measurements of H_2O_2 to predictions from a photochemical steady-state box model. The box model contains all expected gas-phase chemistry affecting the hydroperoxide budget, but lacks any physical parameters such as transport, dry deposition, or wet scavenging. The box model severely over-predicts H_2O_2, particularly in the lower troposphere below 3–4 km altitude where the model on average predicts 2–4 times higher mixing ratios of H_2O_2 than are measured (Figure 4) and this under-prediction

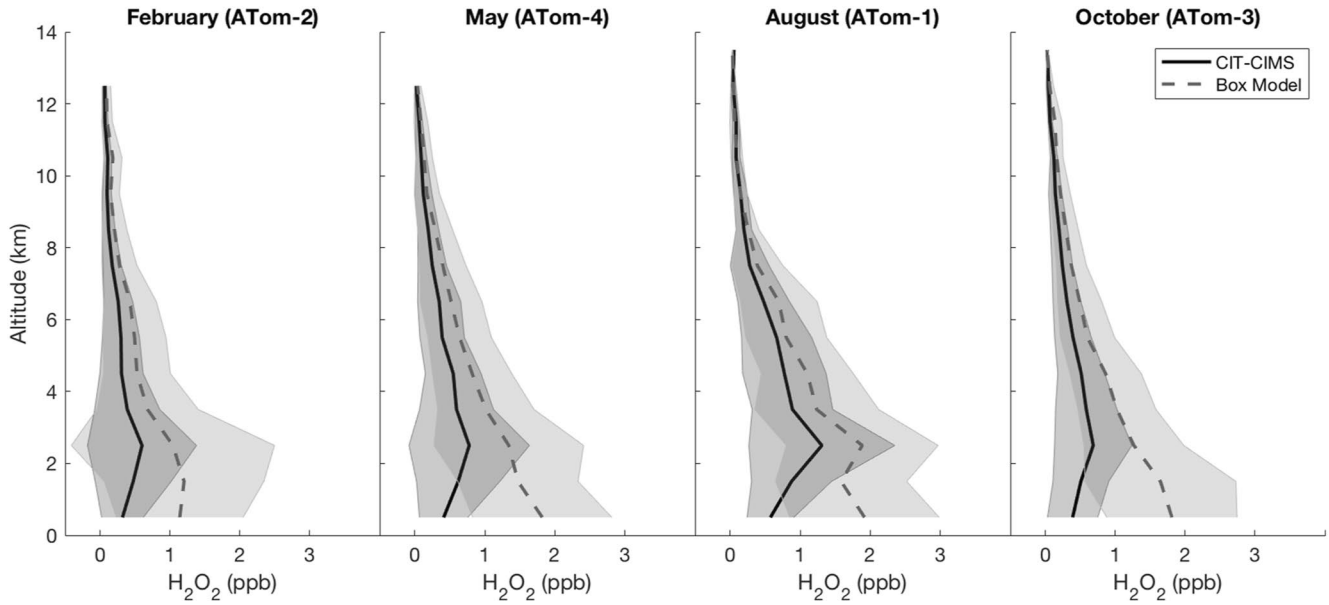

Figure 4. Comparison of H_2O_2 mixing ratios from measurements (CIT-CIMS) and those following chemical relaxation over 5 days after the measurements calculated using a photochemical box model. Throughout the lower troposphere, H_2O_2 mixing ratios are less than half of their steady state values, reflecting the importance of loss via wet and dry deposition. The results are averaged over 1 km altitude bins and shaded region represent one standard deviation of the mean.

is consistent across time of year. Assuming the model captures H_2O_2 photochemical production and loss correctly and that the model has reached steady-state with respect to H_2O_2, the observed over-prediction by the model is likely a result of a missing NPL term. Given that deposition is expected to comprise a significant portion of H_2O_2 loss, this missing loss term likely reflects the lack of this term in the model. In addition, MHP is less likely to undergo depositional loss and does not exhibit the same measurement–model disparity at low altitudes (Figure S2 in Supporting Information S1). Here, we use the difference between instantaneous daylight measurements and the box model to infer the magnitude of the missing loss rate and therefore the expected rate of H_2O_2 deposition. Assuming steady-state, the difference between the model and the measurements can be expressed as

$$\left[H_2O_2\right]_{\text{mod}} - \left[H_2O_2\right]_{\text{meas}} = \frac{P}{L} - \frac{P}{L + \text{NPL}} \tag{10}$$

$$\text{NPL} = L\left(\frac{\left[H_2O_2\right]_{\text{model}}}{\left[H_2O_2\right]_{\text{meas}}} - 1\right) \tag{11}$$

where NPL is the missing loss rate (s^{-1}) needed to reconcile the model with the measurements, L is the H_2O_2 photochemical loss term, and P is the H_2O_2 production term (from $HO_2 + HO_2$ chemistry). For the marine boundary layer, in assigning all of the NPL to dry deposition, the deposition velocity can be estimated as:

$$V_d = \text{NPL} \times \text{BLH} \tag{12}$$

where BLH is the marine boundary layer height.

Figure 5 indicates the estimated non-photochemical first-order loss for each deployment averaged over altitude and latitude calculated from Equation 11. As expected from Figure 4, the loss rate is highest at low altitudes and decreases with increasing altitude. Within the boundary layer, the average NPL is $(11 \pm 3) \times 10^{-6}$ s^{-1} and varies considerably depending on the month sampled (e.g., highest in August and lowest in October). From the model, the average total photochemical loss rate is on order of $(12 \pm 6) \times 10^{-6}$ s^{-1} in the boundary layer, hence physical loss is highly competitive in the lower atmosphere and is estimated to result in the majority of H_2O_2 loss. Above 8 km the NPL rate declines to close to zero, indicating that the loss at these altitudes is primarily photochemical and that the UTLS is closer to photochemical steady-state. The NPL rate also shows some latitudinal dependence (Figure 5). The loss is highest in the tropics and subtropical latitudes and declines moving poleward. A low NPL

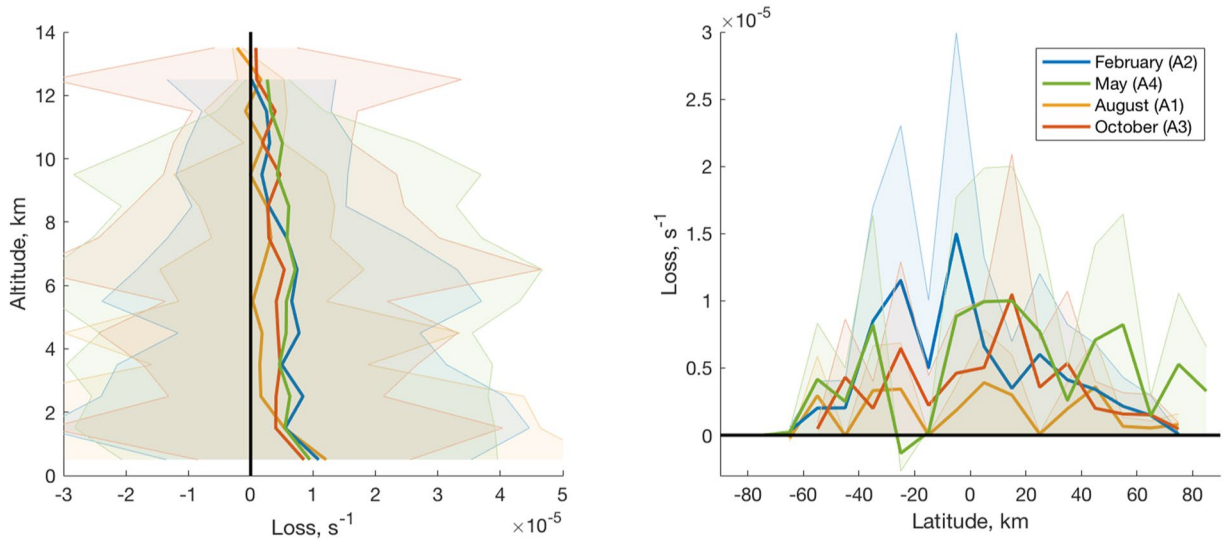

Figure 5. Calculation of the H_2O_2 non-photochemical loss rate averaged over altitude (left, includes all latitudes) and latitude (right, includes all altitudes) for each deployment. The apparent loss was found by comparing the ATom measurements to the predictions by a photochemical box model and attributing the difference to a missing deposition loss term in the model. A1–A4 refer to the four different ATom deployments. Shading represents one sigma standard deviation of the mean.

rate in the subtropics (20°–30°) suggests the influence of dry downwelling air in this region that is much closer to steady-state. Similarly, the poles show an average NPL rate that is close to zero, suggesting that, on average, physical losses are not as important as photochemistry in these regions.

Assuming that deposition to the ocean dominates the derived NPL term, we can estimate the depositional velocity in the lower atmosphere, which depends upon the H_2O_2 loss rate and the height of the marine boundary layer. Because the regions in which NPL is close to zero, such as occurs at high latitudes (Figure 5), likely have other processes beyond dry deposition contributing to peroxide loss, the deposition velocity is only calculated using data from −30° to 30° latitudes and for altitudes less than the estimated MBL (modeled via GEOS5). Equation 12 gives median (mean ± standard deviation) depositional velocities of 1.2 (1.7 ± 2.0), 1.3 (1.3 ± 2.2), 1.2 (2.5 ± 5.4), and 1.0 (1.5 ± 2.0) cm s^{-1} for the marine boundary layer average in February, May, August, and October, respectively. These velocities correspond to median (mean ± standard deviation) wind speeds of 11 (17 ± 17), 8.4 (8.5 ± 3.3), 8.6 (8.3 ± 2.5), and 6.4 (11.4 ± 9.3) m s^{-1}, respectively, within the same latitude and altitude region. Previous estimates, conducted by comparing airborne or ship-based measurements with Lagrangian, chemical box, or global circulation models (EMAC), found a rate between 0.5 and 1.8 cm s^{-1} at wind speeds of 5–10 m s^{-1} (Fischer et al., 2015; Stickler et al., 2007). Hence the calculated deposition velocities in this study are within the range of previously estimated values. These studies note that the deposition rate primarily depends upon the transfer velocity of H_2O_2 to the ocean surface, which is determined by wind speed, rather than other parameters such as ocean uptake resistance. However, other factors not accounted for in this analysis may impact the calculated deposition velocity. Entrainment of H_2O_2 from aloft, for example, will lead to an underestimation of the H_2O_2 deposition velocity by providing an unaccounted source of H_2O_2 in the observations (for example, Q. Li et al., 2003; Singh et al., 2003). The effect of entrainment on the deposition calculation presented here is evaluated in Supporting Information S1.

Because H_2O_2 deposition represents a permanent loss from the atmosphere, this loss is net oxidant consuming. A H_2O_2 deposition rate of (8–12) × 10^{-6} s^{-1} results in an average net loss of 80 ppt H_2O_2 per day for median boundary layer H_2O_2 mixing ratios (400 ppt). Combined with H_2O_2 loss due to OH, this results in an average loss of 300 ppt HO_x per day in the remote marine boundary layer. To assess the total magnitude of this H_2O_2 deposition on HO_x, GEOS-Chem was run with zero H_2O_2 deposition and with the current ("standard", see the Supporting Information) H_2O_2 deposition rate doubled. The standard run predicts H_2O_2 dry deposition velocities of 0.5–1.5 cm s^{-1}, with an average of 1.18 cm s^{-1} that gives a predicted H_2O_2 lifetime of 23.5 hr against dry deposition (assuming 1 km MBL height). Doubling the standard H_2O_2 deposition rate decreases boundary layer H_2O_2 by 10%–40% and provides a closer match to observed H_2O_2 mixing ratios at lower altitudes (<1 km altitude) for

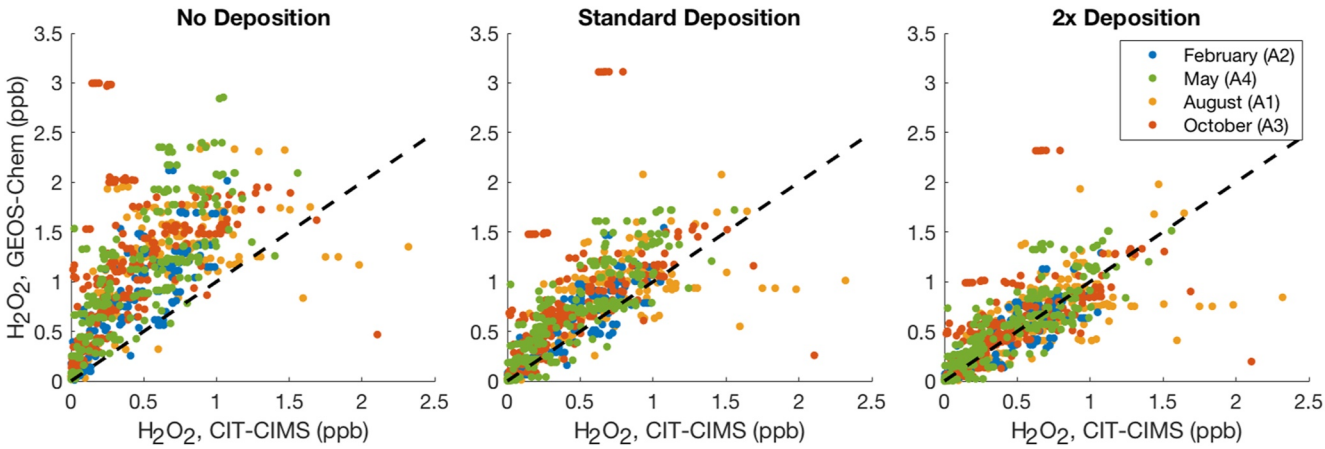

Figure 6. Correlation between CIT-CIMS measured and Goddard Earth Observing System-Chem simulated H_2O_2 mixing ratios for different model deposition velocities in the non-polar remote marine boundary layer (altitudes <1 km and latitudes between −60° and 60°). Doubling the H_2O_2 deposition rate (right) in the model provides a closer match to observed H_2O_2 mixing ratios below 1 km altitude. The RMS error averaged across deployments for each simulation type is 0.78 for no deposition, 0.39 for the standard deposition, and 0.30 for 2× deposition. The dashed line indicates a 1:1 (perfect) comparison.

latitudes between −60° and 60° (Figure 6). However, note that GEOS-Chem does generally over-predict H_2O_2 at all altitudes, not just within the MBL (see Section 3.3 and Figure S5 in Supporting Information S1), and thus increasing the deposition rate may be helping compensate for an issue in the photochemical production or loss of H_2O_2 in GEOS-Chem that exists at all altitudes. With this increased deposition, H_2O_2 mixing ratios in the boundary layer in GEOS-Chem are up to 2.5–4 times lower than their value in the no deposition run and result in a 5%–10% decrease (depending on season) in total HO_x, indicating the importance of H_2O_2 deposition as a HO_x sink in the marine boundary layer (Figure 7). These losses are especially important at the equator and in the southern mid-latitudes (40°–60°) in February and October and prevalent in the equatorial to northern mid-latitudes (40°–60°) and northern pole (>80°) in May and August, following the pattern in seasonal distributions of sunlight and rain. Both the Atlantic and Pacific Ocean basins have a very similar distribution in the change in HO_x.

3.3. MHP Transport via Convective Activity

Correlations between GEOS-Chem and the measurements across the whole deployment (shown in Supporting Information S1) for H_2O_2 indicate generally good agreement between the two, although the model does systematically over-predict H_2O_2. In particular, the months of August (ATom-1) and May (ATom-4) produce correlations between the model and the measurements with slopes of 1.03 and 1.05 with R^2 values of 0.69 and 0.72, respectively; the bias increases in February and October, with slopes of 1.13 and 1.18, respectively (measurement

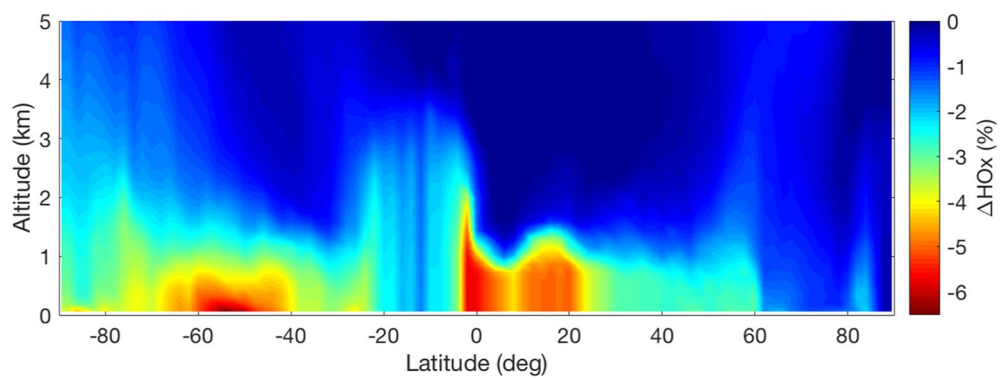

Figure 7. Effect of H_2O_2 deposition on HO_x in the Atlantic remote marine boundary layer during the October (ATom-3) deployment. Total HO_x in the boundary layer declines by 1%–5% in the high deposition simulation compared to when deposition is not included, and particularly affects the equatorial and mid-latitudes (40°–60°) suggesting this is where H_2O_2 deposition is most important.

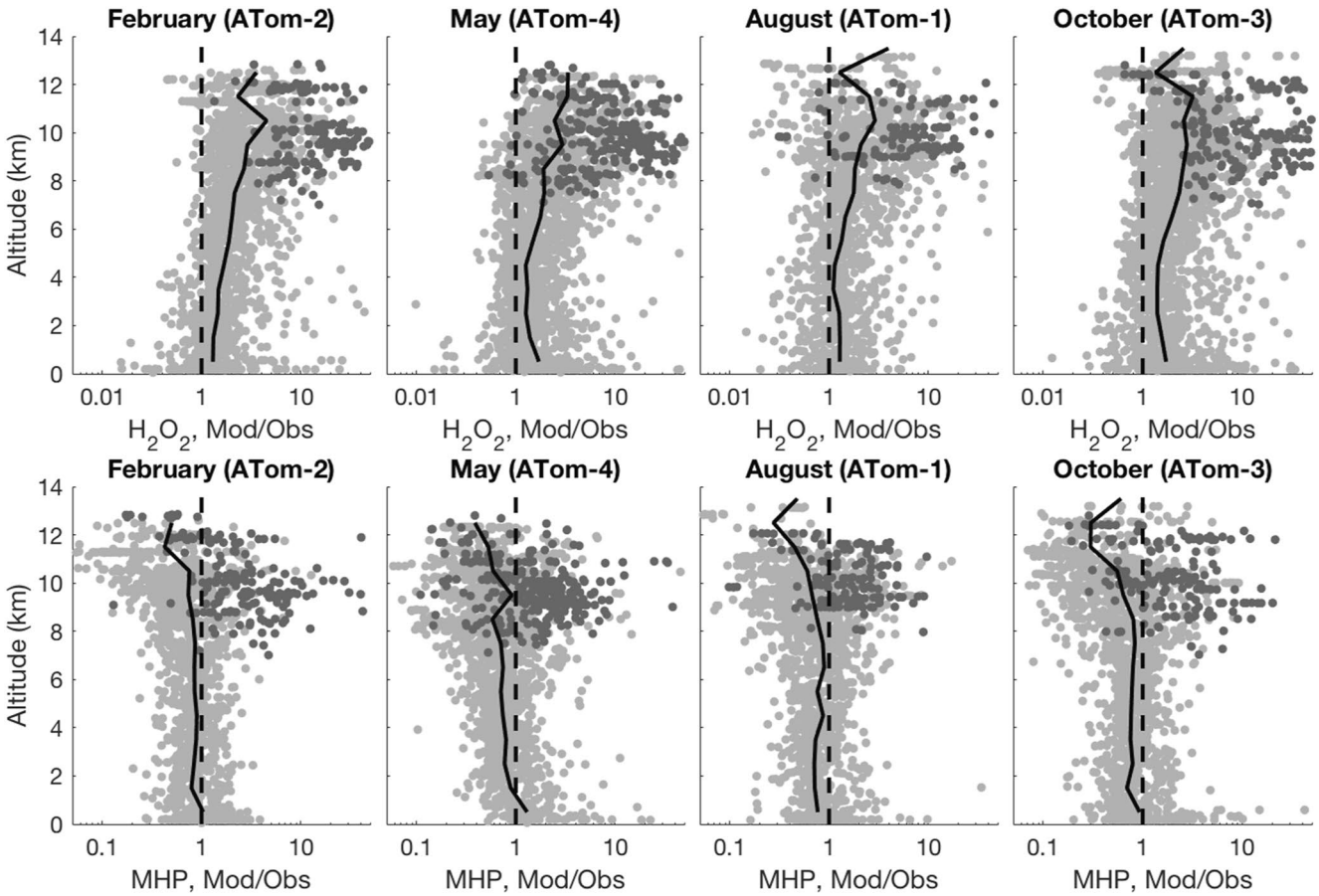

Figure 8. Ratio of measured ("obs") H_2O_2 (top row) and methyl hydroperoxide (bottom row) with that predicted by Goddard Earth Observing System (GEOS)-Chem ("mod") as a function of altitude. Lighter points were collected in the troposphere and darker points were collected in the lower stratosphere, as determined by O_3 measurements above 100 ppbv for altitudes above 7 km. The solid line indicates the median value for all points in 1 km altitude bins and the dashed line represents 1:1 or prefect correlation between the model and the measurements. GEOS-Chem systematically over-predicts H_2O_2 and under-predicts MHP relative to the measurements at all altitudes, with the discrepancy most severe at altitudes above 8 km.

uncertainty is 30%). However, this agreement worsens in the UTLS as indicated in Figure 8, which depicts the ratio of measured H_2O_2 and MHP to that predicted by GEOS-Chem. Above 8 km, the average ratio of the model to measurements ranges between 2 and 4, depending on season and altitude, and the model may be as much as 10 times higher than the measurements in the lower stratosphere. This ratio corresponds to an absolute difference of several tens of pptv: observed H_2O_2 above 8 km altitude is in the range of <1–600 pptv with a mean 95 ± 100 pptv while GEOS-Chem predicts 10–900 pptv with a mean of 210 ± 170 (averaged across all four deployments). GEOS-Chem more accurately captures the hydroperoxide precursor, HO_2, though does under-predict HO_2 at the highest (above 10 km) and lowest altitudes (below 2 km), relative to measurements. Above an altitude of 10 km, GOES-Chem over-predicts HO_2 by a factor of about 2, corresponding to an absolute difference of about 5–10 pptv (see, for example, Brune, Miller, Thames, et al., 2019). By comparison, the photochemical box model more accurately captures H_2O_2 at high altitudes and is an factor of 1–2 times higher on average (absolute difference of 20–40 pptv) than the measurements (Figure 4). That GEOS-Chem has a higher over-prediction than the box model suggests that GEOS-Chem contains an additional source of H_2O_2 in the UTLS not present in the box model nor in the atmosphere as sampled during ATom.

The model and the measurements are less well correlated for MHP than for H_2O_2 across the deployment as a whole. Correlations between the model and the measurements for MHP are best in February (ATom-2) and October (ATom-3), which both give slopes of 0.58 with R^2 values of 0.65 and 0.75, respectively; in comparison, August and May give slopes of 0.57 and 0.49 (see Supporting Information S1). This model under-prediction is most evident in the UTLS, where the median ratio of GEOS-Chem to the measurements is between 0.3 and 0.7

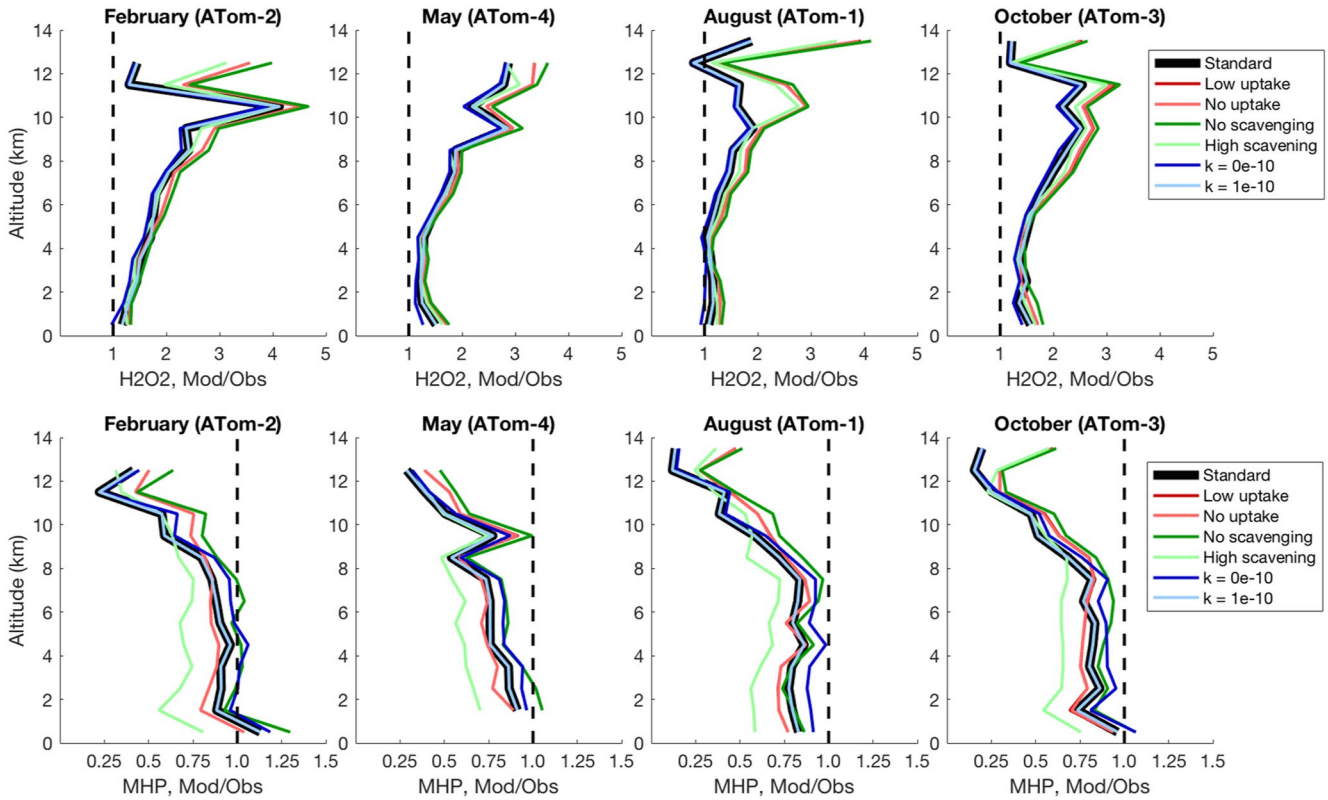

Figure 9. Ratio of measured ("obs") and Goddard Earth Observing System (GEOS)-Chem predicted ("mod") H_2O_2 (top row) and MHP (bottom row) shown as the median when averaged over altitude for several different model configurations. Standard refers to the current GEOS-Chem configuration; low and no uptake refers to alterations to the HO_2 uptake coefficient (γ); No and high scavenging refers to MHP wet deposition; and k refers to the $CH_3OO + OH$ rate coefficient. Despite improvements in the lower troposphere, these alterations do not improve measurement and model correlation in the UTLS. The dashed line represents 1:1 or prefect correlation between the model and the measurements.

with an average of 0.50 ± 0.14 at altitudes above 8 km (Figure 8). The difference between GEOS-Chem and the observations corresponds a significant difference in absolute values, with MHP observations above 8 km in the range of <1–1,000 pptv and an average of 190 ± 220 pptv while GEOS-Chem predicts a range of 1–500 pptv and an average of 80 ± 80 pptv (averaged across all deployments). Similarly, the photochemical box model under-predicts MHP in the UTLS, though the under-prediction is more severe than GEOS-Chem. Above 8 km altitude, the median ratio of the box model to the measurements ranges from 0.13 to 0.55 with an average factor of 0.33 ± 0.16 (Figure S4 in Supporting Information S1). Hence the skill of GEOS-Chem and the box model in reproducing observed H_2O_2 and MHP mixing ratios in the remote atmosphere depends upon the altitude in question, suggesting there is a source of MHP in the atmosphere that is not accurately represented in the models.

Several factors were investigated in GEOS-Chem to determine if they could account for the discrepancy between the model and the measurements including altering the rate of HO_2 loss on heterogeneous surfaces, the rate of $CH_3OO + OH$, and the wet scavenging of MHP (Figure 9). The standard GEOS-Chem configuration here uses a reactive uptake coefficient (γ) of 0.2 for HO_2 onto aerosol surfaces with no products of note formed (O_2 as the sole product). However, several studies have proposed γ values for HO_2 that span two orders of magnitude from 0.01 to 1 (George et al., 2013; Mao et al., 2010; J. Thornton & Abbatt, 2005; J. A. Thornton et al., 2008). To test the effect of decreasing γ, GEOS-Chem was run with $\gamma = 0.07$ ("low uptake") and $\gamma = 0$ ("no uptake") (see the Supporting Information for further discussion of the HO_2 uptake coefficient). Considerable uncertainty also exists in the estimates of the efficiency of MHP scavenging (ranging from 5% to 84%) and a too high scavenging factor may lead to more efficient hydroperoxide removal than exists in the atmosphere (Barth et al., 2001, 2016; Hottmann et al., 2020; Mari et al., 2000). To test the sensitivity of the calculated MHP concentrations to scavenging, two additional simulations with GEOS-Chem were conducted with either no uptake ("no scavenging") and with enhanced uptake ("high scavenging"). Finally, several rate constants for the $CH_3OO + OH$ reaction

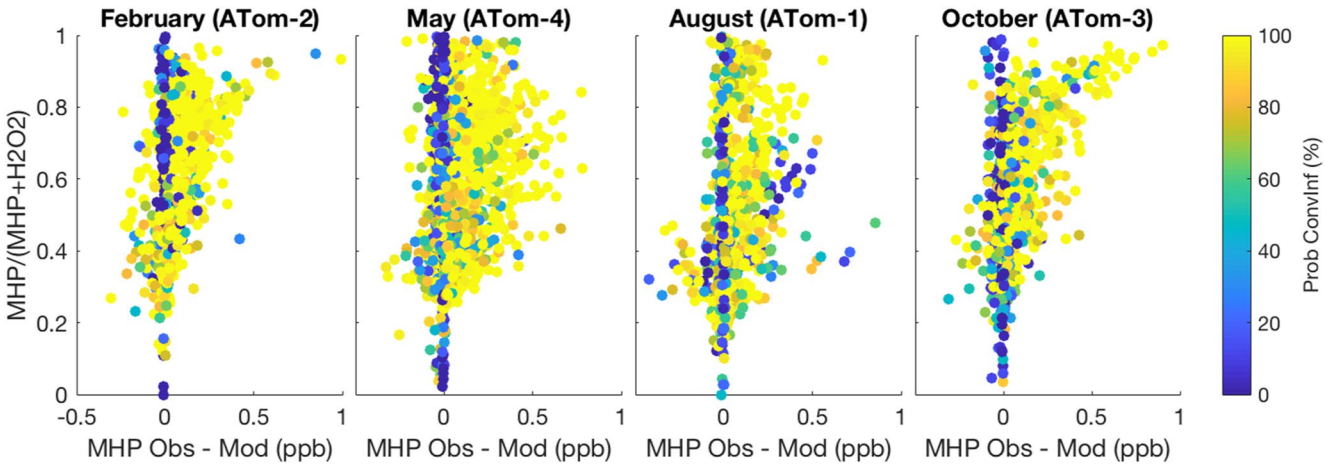

Figure 10. Difference between measured (CIT-CIMS, "obs") and modeled (Goddard Earth Observing System [GEOS]-Chem, "mod") MHP compared with the measured MHP fraction of the hydroperoxide budget (MHP/(MHP + H_2O_2)) and colored by the predicted probability of convective influence (Prob ConvInf). Data shown is from above 5 km altitude. GEOS-Chem deviates most from the measurements at high MHP fraction and when there is a high probability of convection.

have been suggested, with 1×10^{-10} cm^3 $molec^{-1}s^{-1}$ as likely the most accurate (Fittschen, 2019). A lower rate constant would increase MPR, thus increasing the formation rate of MHP. Here, GEOS-Chem was run with $k = 0 \times 10^{-10}$ cm^3 $molec^{-1}s^{-1}$ ("k = 0e−10") and with $k = 1 \times 10^{-10}$ cm^3 $molec^{-1}s^{-1}$ ("k = 1e−10"). Altering these parameters can produce better agreement between the model and the measurements in certain portions of the atmosphere. For example, MHP mixing ratios increase by a significant fraction (>50%) in the polar lower troposphere in the case of no MHP water uptake (see Supporting Information). However, altering these parameters has only minor effects above 8 km altitudes and is not enough to account for the discrepancy between the model and the measurements in the UTLS. Note that GEOS-Chem also does not accurately capture NO and related compounds relative to measurements (Travis et al., 2020), leading to potential discrepancy in the oxidation chemistry in this portion of the atmosphere.

The discrepancy between the measurements and GEOS-Chem in predicting the mixing ratios of both H_2O_2 and MHP in the UTLS likely stems from the model's inability to accurately simulate the influence of convective activity. For altitudes above 5 km, the difference between measured MHP and GEOS-Chem predicted MHP correlates strongly with a high MHP/(MHP + H_2O_2) (Figure 10). The MHP/(MHP + H_2O_2) ratio is used as a tracer for recent convective influence due to the difference in solubilities of these two compounds, where H_2O_2 is preferentially lost due to wet scavenging during convective events. Further confirming the influence of convective activity, the model deviations and MHP fraction are compared to an estimation of the probability of convective influence based on a 10-day back trajectory analysis using the National Centers for Environmental Predictions (NCEP) Global Forecast System (GFS) meteorology (Bowman, 1993; Bowman and Carrie, 2002; see Supporting Information S1 for further details). The convective influence probability is calculated based on the coincidence of the air parcel with clouds, high RH (above 50%), and cloud water. This metric also indicates that GEOS-Chem more accurately captures measured MHP at times when there is very little to no probability of convective influence and less accurately during times of high probability of convective influence (Figure 10). Studies have noted problems in the parameterization of tracer mass fluxes during convection in chemical transport models (Lawrence & Rasch, 2005; Zhang et al., 2021). Comparison to the ATom hydroperoxide data in the UTLS suggests that this treatment of convective mass fluxes in GEOS-Chem merits further investigation and that the peroxide data reported here is a useful diagnostic of these fluxes.

The importance of convection in influencing the chemistry of the UTLS is estimated using the chemistry of MHP/(MHP + H_2O_2) as a tracer for air mass age following convection. This estimation was done using the method outlined in Bertram et al. (2007) for the tropical and subtropical portion (latitudes between −30° and 30°) of ATom. Briefly, a diurnal photochemical steady-state model was initiated with a high MHP/(MHP + H_2O_2) ratio and a high $NO_x/(NO_x + HNO_3)$ ratio, simulating conditions found immediately following convection. This model assumes that HNO_3 and H_2O_2 are scrubbed with near unit efficiency during convection and the model neglects dilution from surrounding background air. The model is initialized with MHP at 1 ppb and NO_x at 2 ppb, with

Table 1
Mean Age[a] (Hours) of Air Mass Encountered at 1 km Altitude Bins From 6 to 12 km, Based on a Comparison of the Measured MHP/(MHP + H_2O_2) Fraction to Modeled Changes in MHP/(MHP + H_2O_2) Fraction Since Convective Influence

	6–7 km	7–8 km	8–9 km	9–10 km	10–11 km	11–12 km
February (ATom-2)	23 ± 4	23 ± 5	26 ± 5	30 ± 8	23 ± 6	25 ± 10
May (ATom-4)	16 ± 4	19 ± 4	23 ± 6	28 ± 7	26 ± 8	21 ± 8
August (ATom-2)	27 ± 6	31 ± 12	37 ± 36	31 ± 7	33 ± 12	43 ± 11
October (ATom-3)	19 ± 2	20 ± 3	23 ± 4	23 ± 6	26 ± 7	24 ± 10

Note. Data are from −30° to 30° latitudes.
[a]Range in values given is the standard deviation in calculated hours since CI for each altitude bin.

H_2O_2 and HNO_3 at near to zero ppt levels; all other species were initiated with their measured concentrations. The model progressed until steady-state was reached (~10 days) and an expression was fit to the change in MHP/(MHP + H_2O_2) and NO_x/(NO_x + HNO_3) over the time between initiation to steady-state in 1 km altitude bins from 6 to 12 km (see Figures S6 and S7 in Supporting Information S1). This expression was then compared to the measured ratios in the same altitude bins to calculate the approximate age of air encountered at the high altitudes in the tropical and subtropical latitude band during the four seasons sampled as part of ATom.

The estimated chemical aging since convective activity for 1 km altitude bins between 6 and 12 km for each deployment is given in Table 1 and Figure S8 in Supporting Information S1. The air mass age ranged from 16 to 43 hr, with the newest air in the lower atmosphere in May and the oldest air in the upper atmosphere in August. Across all four deployments, the average age in the lower region (6–7 km) is 21 hr and this age increases to 28 hr in the upper atmosphere (11–12 km). Note that the neglect of background air mixing likely biases the air mass age to lower values because dilution will lower the MHP mixing ratio and therefore decrease the MHP/H_2O_2 ratio. These ages are similar to those estimated by Bertram et al. (2007), using the same method over North America during summer 2004, who found nearly 50% of the air mass sampled had been convectively influenced within the previous day and 75% within the previous 5 days. This age is faster than suggested by comparison to air mass age calculated using back trajectory analysis, which gives an air mass age in the range of 67–115 hr with the most recently influenced air in the upper troposphere (10–11 km) and the air in the mid-troposphere (6–7 km) less recently influenced, likely due to the difference between physical and chemical aging (the latter primarily occurs only during sunlit hours). These results indicate the wide-spread influence of convection on the chemistry of UTLS with important implications for the chemistry occurring there. Because MHP transports HO_x to the typically low HO_x UTLS, wide-spread convection of MHP increases HO_x in a region with generally higher NO levels and therefore increases O_3 formation in the UTLS (Jaeglé et al., 1997).

4. Conclusions

The observations of hydroperoxides collected during the ATom Mission indicate how these hydroperoxides impact the global oxidative budget of the atmosphere. H_2O_2 is primarily formed at lower altitudes in the tropics due to the HO_2 self-reaction and primarily lost via photolysis in the same region. Globally, OH reaction comprises an average of 30%–35% of H_2O_2 photochemical loss, but this ratio is higher (40%–45%) at lower altitudes and decreases in the UTLS (reaching 20%–25% of loss). Similarly, the ATom data indicate that production of MHP from CH_3OO + HO_2 globally is about 30% of CH_3OO loss relative to NO, with a sharp gradient between the lower and upper atmosphere with the UTLS dominated by CH_3OO + NO chemistry. Loss to OH accounts for a higher fraction of the MHP photochemical loss budget, with a global average of 68%–74%, than for the H_2O_2 budget. Photolysis is net oxidant conserving while reaction with OH and deposition are net oxidant consuming, thus regions like the tropical marine boundary layer which have high hydroperoxide losses to OH reaction and deposition are oxidant consuming.

In addition to photochemical loss, these hydroperoxides affect HO_x due to their physical loss and transport mechanisms. For H_2O_2 within the marine boundary layer, a physical loss on order of (8–12) × 10^{-6} s^{-1} is needed to reconcile predictions from a photochemical steady-state model with observations of H_2O_2 made during ATom.

This loss rate corresponds to a mean deposition velocity of 1.0–1.3 cm s^{-1}, assuming wet deposition does not contribute as is likely the case for ATom given that the aircraft generally minimized sampling in the boundary layer when it was cloudy. When combined with loss to OH reaction in the boundary layer, these values correspond to a removal of 300 ppt HO_x per day, estimated by the GEOS-Chem in the standard deposition configuration to reduce total HO_x in the remote marine boundary layer by 5%–10%. Increasing the GEOS-Chem H_2O_2 deposition rate to twice its default value provides a better match to H_2O_2 observations and results in an additional 1.5% decline in boundary layer HO_x.

Similarly, in the upper troposphere, GEOS-Chem systematically over-predicts H_2O_2 and under-predicts MHP relative to ATom measurements in all seasons, with these deviations reaching a factor of up to 10–100 times difference. Sensitivity tests of HO_2 loss to heterogeneous surfaces, MHP wet deposition treatment, and reducing the rate of CH_3OO + OH in the model show that altering these parameters can somewhat reduce model and measurement differences in the troposphere. However, altering these parameters even to extreme values does not reconcile GEOS-Chem with the ATom measurements within the upper atmosphere. Correlation with tracers of recent convective activity suggest that much of the under-prediction of MHP and over-prediction of H_2O_2 in GEOS-Chem likely reflects error in the convective mass flux. Given the importance of MHP as a source of HO_x in the UTLS and the prevalence of convectively influenced air in this region (most sampled air masses in the equatorial UTLS, e.g., had been convectively influenced within the previous 5 days), more work is needed to address this issue.

Data Availability Statement

The field data collected during the ATom deployments and used in this paper are available at https://doi.org/10.3334/ORNLDAAC/1581.

Acknowledgments
Funding for this work was provided by NASA Grant No. NNX15AG61A. Additional support for H. M. Allen was provided by the National Science Foundation Graduate Research Fellowship under Grant No. DGE-1144469 and additional support for M. J. Kim was provided by the National Science Foundation Grant No. 1524860. The authors would like to thank the organizers of the ATom Mission, particularly S. C. Wofsy and T. B. Ryerson, for providing the opportunity to gather these data. We would also like to thank E. Czech, D. Jordan, and the people at ESPO, as well as the pilots and crew of the DC-8 for the infrastructural support that made these measurements possible.

References

Allen, H. M., Crounse, J. D., Kim, M. J., Tang, A. P., Ray, E. A., McKain, K., & Wennberg, P. O. (2021). H_2O_2 and CH_3OOH (MHP) in the remote atmosphere. I: Global distribution and regional influences. *Journal of Geophysical Research: Atmospheres*.

Allen, H. M., Crounse, J. D., Kim, M. J., Teng, A. P., & Wennberg, P. O. (2019). *ATom: L2 in situ data from Caltech chemical ionization mass spectrometer (CIT-CIMS)*. ORNL DAAC. https://doi.org/10.3334/ORNLDAAC/1713

Anglada, J. M., Crehuet, R., Martins-Costa, M., Francisco, J. S., & Ruiz-López, M. (2017). The atmospheric oxidation of CH_3OOH by the OH radical: The effect of water vapor. *Physical Chemistry Chemical Physics*, *19*, 12331–12342. https://doi.org/10.1039/c7cp01976a

Apel, E. C., Asher, E. C., Hills, A. J., & Hornbrook, R. S. (2019). *ATom: L2 volatile organic compounds (VOCs) from the trace organic gas analyzer (TOGA)*. ORNL DAAC. https://doi.org/10.3334/ORNLDAAC/1749

Atkinson, R., Baulch, D. L., Cox, R. A., Crowley, J. N., Hampson, R. F., Hynes, R. G., et al. (2006). Evaluated kinetic and photochemical data for atmospheric chemistry: Volume II—Gas phase reaction of organic species. *Atmospheric Chemistry and Physics*, *6*, 3625–4055. https://doi.org/10.5194/acp-6-3625-2006

Barth, M. C., Bela, M. M., Fried, A., Wennberg, P. O., Crounse, J. D., Clair, S. J. M., et al. (2016). Convective transport and scavenging of peroxides by thunderstorms observed over the central U.S. during DC3. *Journal of Geophysical Research: Atmospheres*, *121*, 4272–4295. https://doi.org/10.1002/2015jd024570

Barth, M. C., Stuart, A. L., & Skamarock, W. C. (2001). Numerical simulations of the July 10, 1996, stratospheric-tropospheric experiment: Radiation, aerosols, and ozone (STERAO)-deep convection experiment storm: Redistribution of soluble tracers. *Journal of Geophysical Research*, *106*, 12381–12400. https://doi.org/10.1029/2001jd900139

Bates, K. H., Jacob, D. J., Wang, S., Hornbrook, R. S., Apel, E. C., Kim, M. J., & Wofsy, S. C. (2021). The global budget of atmospheric methanol: New constraints on secondary, oceanic, and terrestrial sources. *Journal of Geophysical Research: Atmospheres*, *126*, e2020JD033439. https://doi.org/10.1029/2020jd033439

Bela, M. M., Barth, M. C., Toon, O. B., Fried, A., Homeyer, C. R., Morrison, H., et al. (2016). Wet scavenging of soluble gases in DC3 deep convective storms using wrf-chem simulations and aircraft observations. *Journal of Geophysical Research: Atmospheres*, *121*, 4233–4257. https://doi.org/10.1002/2015jd024623

Bela, M. M., Barth, M. C., Toon, O. B., Fried, A., Ziegler, C., Cummings, K. A., et al. (2018). Effects of scavenging, entrainment, and aqueous chemistry on peroxides and formaldehyde in deep convective outflow over the central and southeastern United States. *Journal of Geophysical Research: Atmospheres*, *123*, 7594–7614. https://doi.org/10.1029/2018jd028271

Bertram, T. H., Perring, A. E., Wooldridge, P. J., Crounse, J. D., Kwan, A. J., Wennberg, P. O., et al. (2007). Direct measurements of the convective recycling of the upper troposphere. *Science*, *315*, 816–820. https://doi.org/10.1126/science.1134548

Bey, I., Jacob, D. J., Yantosca, R. M., Logan, J. A., Field, B. D., Fiore, A. M., et al. (2001). Global modeling of tropospheric chemistry with assimilated meteorology: Model description and evaluation. *Journal of Geophysical Research*, *106*, 23073–23095. https://doi.org/10.1029/2001jd000807

Bian, H., & Prather, M. J. (2002). Fast-j2: Accurate simulation of stratospheric photolysis in global chemical models. *Journal of Atmospheric Chemistry*, *41*, 281–296. https://doi.org/10.1023/a:1014980619462

Bowman, K. P. (1993). Large-scale isentropic mixing properties of the Antarctic polar vortex from analyzed winds. *Journal of Geophysical Research: Atmospheres*, *98*, 23013–23027. https://doi.org/10.1029/93jd02599

Bowman, K. P., & Carrie, G. D. (2002). The mean-meridional transport circulation of the troposphere in an idealized GCM. *Journal of the Atmospheric Sciences*, *59*, 1502–1514. https://doi.org/10.1175/1520-0469(2002)059<1502:tmmtco>2.0.co;2

Bozem, H., Pozzer, A., Harder, H., Martinez, M., Williams, J., Lelieveld, J., & Fischer, H. (2017). The influence of deep convection on HCHO and H_2O_2 in the upper troposphere over Europe. *Atmospheric Chemistry and Physics*, *17*, 11835–11848. https://doi.org/10.5194/acp-17-11835-2017

Brune, W. H., Miller, D. O., & Thames, A. B. (2019). *ATom: L2 measurements from airborne tropospheric hydrogen oxides sensor (ATHOS)*. ORNL DAAC. https://doi.org/10.3334/ORNLDAAC/1709

Brune, W. H., Miller, D. O., Thames, A. B., Allen, H. A., Apel, E. C., Blake, D. R., & Wolfe, G. M. (2019). Exploring oxidation in the remote free troposphere: Insights from Atmospheric Tomography (ATom). *Journal of Geophysical Research: Atmospheres*, *125*, e2019JD031685.

Burkholder, J. B., Sander, S. P., Abbatt, J., Barker, J. R., Huie, R. E., Kolb, C. E., & Wine, P. H. (2015). *Chemical kinetics and photochemical data for use in atmospheric studies, evaluation no. 18*. Pasadena: Jet Propulsion Laboratory. (JPL publication 15-10).

Chang, W., Lee, M., & Heikes, B. G. (2004). One-dimensional photochemical study of H_2O_2, CH_3OOH, and HCHO in the marine boundary layer during Pacific Exploratory Mission in the Tropics (PEM-Tropics) B. *Journal of Geophysical Research*, *109*, D06307. https://doi.org/10.1029/2003jd004256

Cohan, D. S., Schultz, M. G., Jacob, D. J., Heikes, B. G., & Blake, D. R. (1999). Convective injection and photochemical decay of peroxides in the tropical upper troposphere: Methyl iodide as a tracer of marine convection. *Journal of Geophysical Research*, *104*, 5717–5724. https://doi.org/10.1029/98jd01963

Cuchiara, G. C., Fried, A., Barth, M. C., Bela, M., Homeyer, C. R., Gaubert, B., & Heath, N. (2020). Vertical transport, entrainment, and scavenging processes affecting trace gases in a modeled and observed SEAC^{4}RS case study. *Journal of Geophysical Research: Atmospheres*, *125*, e2019JD031957. https://doi.org/10.1029/2019jd031957

Diskin, G. S., & DiGangi, J. P. (2019). *ATom: L2 in situ atmospheric water vapor from the diode laser hygrometer (DLH)*. ORNL DAAC. https://doi.org/10.3334/ORNLDAAC/1710

Elkins, J. W., Hintsa, E., & Moore, F. (2019). ATom DC-8 GCECD files. NASA ESPO, online. Retrieved from https://espo.nasa.gov/atom/archive/browse/atom/DC8/GCECD

Fischer, H., Pozzer, A., Schmitt, T., Jöckel, P., Klippel, T., Taraborrelli, D., & Lelieveld, J. (2015). Hydrogen peroxide in the marine boundary layer over the South Atlantic during the OOMPH cruise in March 2007. *Atmospheric Chemistry and Physics*, *15*, 6971–6980. https://doi.org/10.5194/acp-15-6971-2015

Fittschen, C. (2019). The reaction of peroxy radicals with OH radicals. *Chemical Physics Letters*, *725*, 102–108. https://doi.org/10.1016/j.cplett.2019.04.002

George, I. J., Matthews, P. S. J., Whalley, L. K., Brooks, B., Goddard, A., Baeza-Romero, M. T., & Heard, D. E. (2013). Measurements of uptake coefficients for heterogeneous loss of HO_2 onto submicron inorganic salt aerosols. *Physical Chemistry Chemical Physics*, *15*, 12829–12845. https://doi.org/10.1039/c3cp51831k

Hall, B. D., & Claiborn, C. S. (1997). Measurements of the dry deposition of peroxides to a Canadian boreal forest. *Journal of Geophysical Research*, *102*, 29343–29353. https://doi.org/10.1029/97jd01113

Hall, S. R., & Ullmann, K. (2019). *ATom: L2 photolysis frequencies from NCAR CCD actinic flux Spectroradiometers (CAFS)*. ORNL DACC. https://doi.org/10.3334/ORNLDAAC/1714

Hanisco, T. F., Hannun, R. A., Clair, S. J. M., & Wolfe, G. M. (2019). *ATom: L2 measurements of in situ airborne formaldehyde (ISAF)*. ORNL DAAC. https://doi.org/10.3334/ORNLDAAC/1730

Harvard, A. C. M. G. (2019). *GEOS-Chem*. Retrieved from http://www.geos-chem.org

Heikes, B. G., Lee, M., Bradshaw, J., Sandholm, S., Davis, D. D., Crawford, J., et al. (1996). Hydrogen peroxide and methylhydroperoxide distributions related to ozone and odd hydrogen over the north pacific in the fall of 1991. *Journal of Geophysical Research*, *101*, 1891–1905. https://doi.org/10.1029/95jd01364

Hottmann, B., Hafermann, S., Tomsche, L., Marno, D., Martinez, M., Harder, H., et al. (2020). Impact of the South Asian monsoon outflow on atmospheric hydroperoxides in the upper troposphere. *Atmospheric Chemistry and Physics*, *20*, 12655–12673. https://doi.org/10.5194/acp-20-12655-2020

Huey, L. G., Nowak, J. B., Tanner, D., & Kim, S. (2019). *ATom: L2 in situ peroxyacetyl nitrate (PAN) measurements from Georgia tech CIMS*. ORNL DAAC. https://doi.org/10.3334/ORNLDAAC/1715

Jaeglé, L., Jacob, D. J., Brune, W. H., Faloona, I., Tan, D., Heikes, B. G., et al. (2000). Photochemistry of HO_x in the upper troposphere at northern midlatitudes. *Journal of Geophysical Research*, *105*, 3877–3892. https://doi.org/10.1029/1999jd901016

Jaeglé, L., Jacob, D. J., Wennberg, P. O., Spivakovsky, C. M., Hanisco, T. F., Lanzendorf, E. J., et al. (1997). Observed OH and HO_2 in the upper troposphere suggest a major source from convective injection of peroxides. *Geophysical Research Letters*, *24*, 3181–3184. https://doi.org/10.1029/97gl03004

Jenkin, M. E., Valorso, R., Aumont, B., & Rickard, A. R. (2019). Estimation of rate coefficients and branching ratios for reactions of organic peroxy radicals for use in automated mechanism construction. *Atmospheric Chemistry and Physics*, *19*, 7691–7717. https://doi.org/10.5194/acp-19-7691-2019

Jobson, B. T., Frost, G. J., McKeen, S. A., Ryerson, T. B., Buhr, M. P., Parrish, D. D., et al. (1998). Hydrogen peroxide dry deposition lifetime determined from observed loss rates in a power plant plume. *Journal of Geophysical Research*, *103*, 22617–22628. https://doi.org/10.1029/98jd01619

Keller, C. A., Long, M. S., Yantosca, R. M., Da Silva, A. M., Pawson, S., & Jacob, D. J. (2014). HEMCO v1.0: A versatile, esmf-compliant component for calculating emissions in atmospheric models. *Geoscientific Model Development*, *7*, 1409–1417. https://doi.org/10.5194/gmd-7-1409-2014

Lawrence, M. G., & Rasch, P. J. (2005). Tracer transport in deep convective updrafts: Plume ensemble versus bulk formulations. *Journal of the Atmospheric Sciences*, *62*, 2880–2894. https://doi.org/10.1175/jas3505.1

Lee, M., Heikes, B. G., & O'Sullivan, D. W. (2000). Hydrogen peroxide and organic hydroperoxide in the troposphere: A review. *Atmospheric Environment*, *34*, 3475–3494. https://doi.org/10.1016/s1352-2310(99)00432-x

Li, Q., Jacob, D. J., Yantosca, R. M., Heald, C. L., Singh, H. B., Koike, M., & Streets, D. G. (2003). A global three-dimensional model analysis of the atmospheric budgets of HCN and CH_3CN: Constraints from aircraft and ground measurements. *Journal of Geophysical Research*, *108*, 8827. https://doi.org/10.1029/2002jd003075

Li, Y., Pickering, K. E., Barth, M. C., Bela, M. M., Cummings, K. A., & Allen, D. J. (2019). Wet scavenging in WRF-Chem simulations of parameterized convection for a severe storm during the DC3 field campaign. *Journal of Geophysical Research*, *124*, 7413–7428. https://doi.org/10.1029/2019jd030484

Lin, S.-J., & Rood, R. B. (1996). Multidimensional flux-form semi-Lagrangian transport schemes. *Monthly Weather Review*, *124*, 2046–2070. https://doi.org/10.1175/1520-0493(1996)124<2046:mffslt>2.0.co;2

Mao, J., Jacob, D. J., Evans, M. J., Olson, J. R., Ren, X., Brune, W. H., et al. (2010). Chemistry of hydrogen oxide radicals (HO_x) in the arctic troposphere in spring. *Atmospheric Chemistry and Physics*, *10*, 5823–5838. https://doi.org/10.5194/acp-10-5823-2010

Mari, C., Jacob, D. J., & Bechtold, P. (2000). Transport and scavenging of soluble gases in a deep convective cloud. *Journal of Geophysical Research*, *105*, 22255–22267. https://doi.org/10.1029/2000jd900211

McKain, K., & Sweeney, C. (2018). ATom DC-8 NOAA-Picarro-CO2-CH4-CO files. NASA ESPO. Retrieved from https://espo.nasa.gov/atom/archive/browse/atom/DC8/NOAA-Picarro-CO2-CH4-CO

Nguyen, T. B., Crounse, J. D., Teng, A. P., Clair, S. J. M., Paulot, F., Wolfe, G. M., & Wennberg, P. O. (2015). Rapid deposition of oxidized biogenic compounds to a temperate forest. *Proceedings of the National Academy of Sciences*, *112*, E392–E401. https://doi.org/10.1073/pnas.1418702112

Niki, H., Maker, P. D., Savage, C. M., & Breltenbach, L. P. (1983). A Fourier transform infrared study of the kinetics and mechanism for the reaction of OH + CH_3OOH. *Journal of Physical Chemistry*, *87*, 2190–2193. https://doi.org/10.1021/j100235a030

O'Sullivan, D. W., Heikes, B. G., Lee, M., Chang, W., Gregory, G. L., Blake, D. R., & Sachse, G. W. (1999). Distribution of hydrogen peroxide and methylhydroperixde over the Pacific and South Atlantic oceans. *Journal of Geophysical Research*, *104*, 5635–5646.

Prather, M. J., & Jacob, D. J. (1997). A persistent imbalance in HO_x and NO_x photochemistry of the upper troposphere driven by deep tropical convection. *Geophysical Research Letters*, *24*, 3189–3192. https://doi.org/10.1029/97gl03027

Ravetta, F., Jacob, D. J., Brune, W. H., Heikes, B. G., Anderson, B. E., Blake, D. R., et al. (2001). Experimental evidence for the importance of convected methylhydroperoxide as a source of hydrogen oxide (HO_x) radicals in the tropical upper troposphere. *Journal of Geophysical Research*, *106*, 32709–32716. https://doi.org/10.1029/2001jd900009

Ryerson, T. B., Thompson, C. R., Peischl, J., & Bourgeois, I. (2019). *ATom: L2 in situ measurements from NOAA nitrogen oxides and ozone (NOyO3) instrument*. ORNL DAAC. https://doi.org/10.3334/ORNLDAAC/1734

Singh, H. B., Salas, L., Herlth, D., Kolyer, R., Czech, E., Viezee, W., & Kondo, Y. (2003). In situ measurements of HCN and CH_3CN over the Pacific Ocean: Sources, sinks, and budgets. *Journal of Geophysical Research*, *108*, 8795. https://doi.org/10.1029/2002jd003006

Snow, J. A., Heikes, B. G., Shen, H., O'Sullivan, D. W., Fried, A., & Walega, J. (2007). Hydrogen peroxide, methyl hydroperoxide, and formaldehyde over North America and the North Atlantic. *Journal of Geophysical Research*, *112*, D12S07. https://doi.org/10.1029/2006jd007746

Stickler, A., Fischer, H., Bozem, H., Gurk, C., Schiller, C., Martinex-Harder, M., et al. (2007). Chemistry, transport and dry deposition of trace gases in the boundary layer over the tropical Atlantic Ocean and the Guyanas during the GABRIEL field campaign. *Atmospheric Chemistry and Physics*, *7*, 3933–3956. https://doi.org/10.5194/acp-7-3933-2007

Stone, D., Whalley, L. K., & Heard, D. E. (2012). Tropospheric OH and HO_2 radicals: Field measurements and model comparisons. *Chemical Society Reviews*, *41*, 6348–6404. https://doi.org/10.1039/c2cs35140d

Thornton, J., & Abbatt, P. D. (2005). Measurements of HO_2 uptake to aqueous aerosol: Mass accommodation coefficients and net reactive loss. *Journal of Geophysical Research*, *110*, D08309. https://doi.org/10.1029/2004jd005402

Thornton, J. A., Jaeglé, L., & McNeill, V. F. (2008). Assessing known pathways for HO_2 loss in aqueous atmospheric aerosols: Regional and global impacts on tropospheric oxidants. *Journal of Geophysical Research*, *113*, D05303. https://doi.org/10.1029/2007jd009236

Travis, K. R., Heald, C. L., Allen, H. M., Apel, E. C., Arnold, S. R., Blake, D. R., et al. (2020). Constraining remote oxidation capacity with ATom observations. *Atmospheric Chemistry and Physics*, *20*, 7753–7781. https://doi.org/10.5194/acp-20-7753-2020

Vaghjiani, G. L., & Ravishankara, A. R. (1989). Kinetics and mechanism of OH reaction with CH_3OOH. *Journal of Physical Chemistry*, *93*, 1948–1959. https://doi.org/10.1021/j100342a050

Walcek, C. J. (1987). A theoretical estimate of O_3 and H_2O_2 dry deposition over the northeast United States. *Atmospheric Environment*, *21*, 2649–2659. https://doi.org/10.1016/0004-6981(87)90196-x

Zhang, B., Liu, H., Crawford, J. H., Chen, G., Fairlie, D., Chambers, S., et al. (2021). Simulation of radon-222 with the GEOS-Chem model: Emissions, seasonality, and convective transport. *Atmospheric Chemistry and Physics*, *21*, 1861–1887. https://doi.org/10.5194/acp-21-1861-2021